

Supporting Information for

Maximizing Pore and Heteroatom Utilization within N, P Co-doped Polypyrrole-derived Carbon Nanotubes for High-performance Supercapacitors

Xinying Luo^{a†}, Qi Yang^{b†}, Yanli Dong^a, Xiaoxiong Huang^b, Debin Kong^b, Bin Wang^b, Huimin Liu^a, Zhichang Xiao^{a*} and Linjie Zhi^b

^aDepartment of Chemistry, College of Science, Hebei Agricultural University, Baoding 071001, People's Republic of China

^bCAS Key Laboratory of Nanosystem and Hierarchical Fabrication, CAS Center for Excellence in Nanoscience, National Center for Nanoscience and Technology, Beijing 100190, People's Republic of China

[†]These authors contributed equally to this work.

*Corresponding author. Email: xiaozhichangcnu@sina.cn

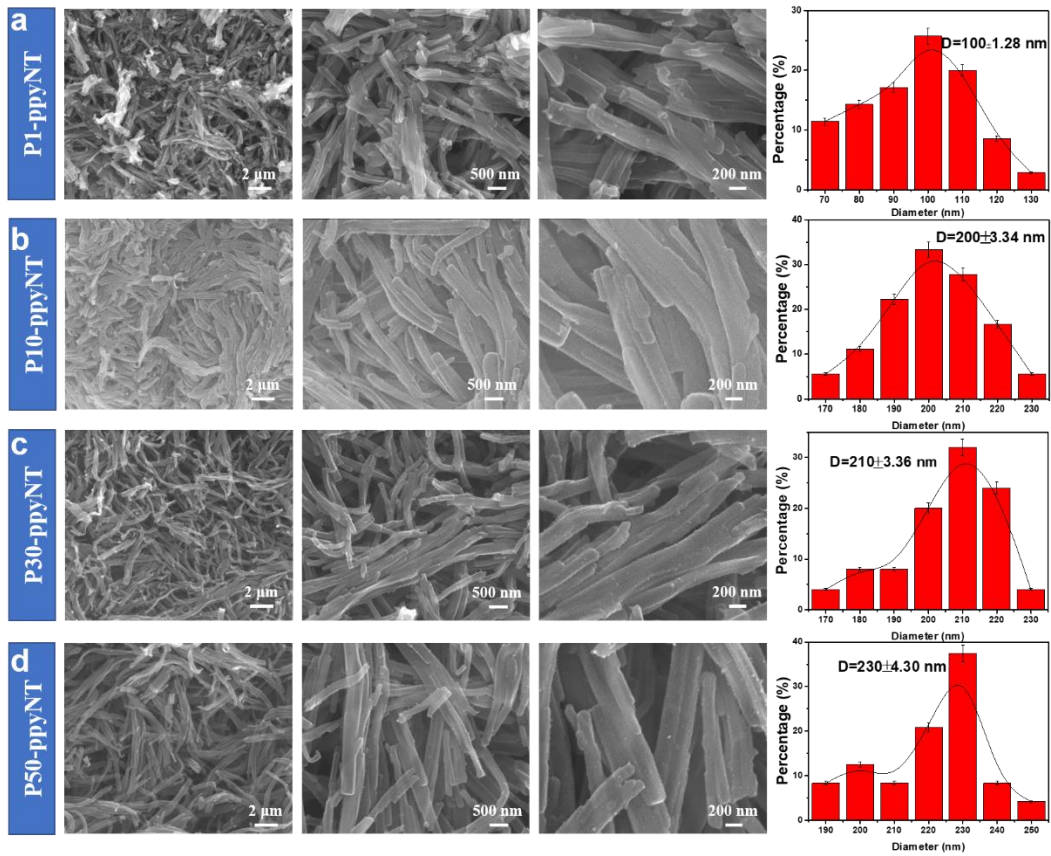


Figure S1. SEM images and diameter count of (a) P1-ppyNT, (b) P10-ppyNT, (c) P30-ppyNT and (d) P50-ppyNT.

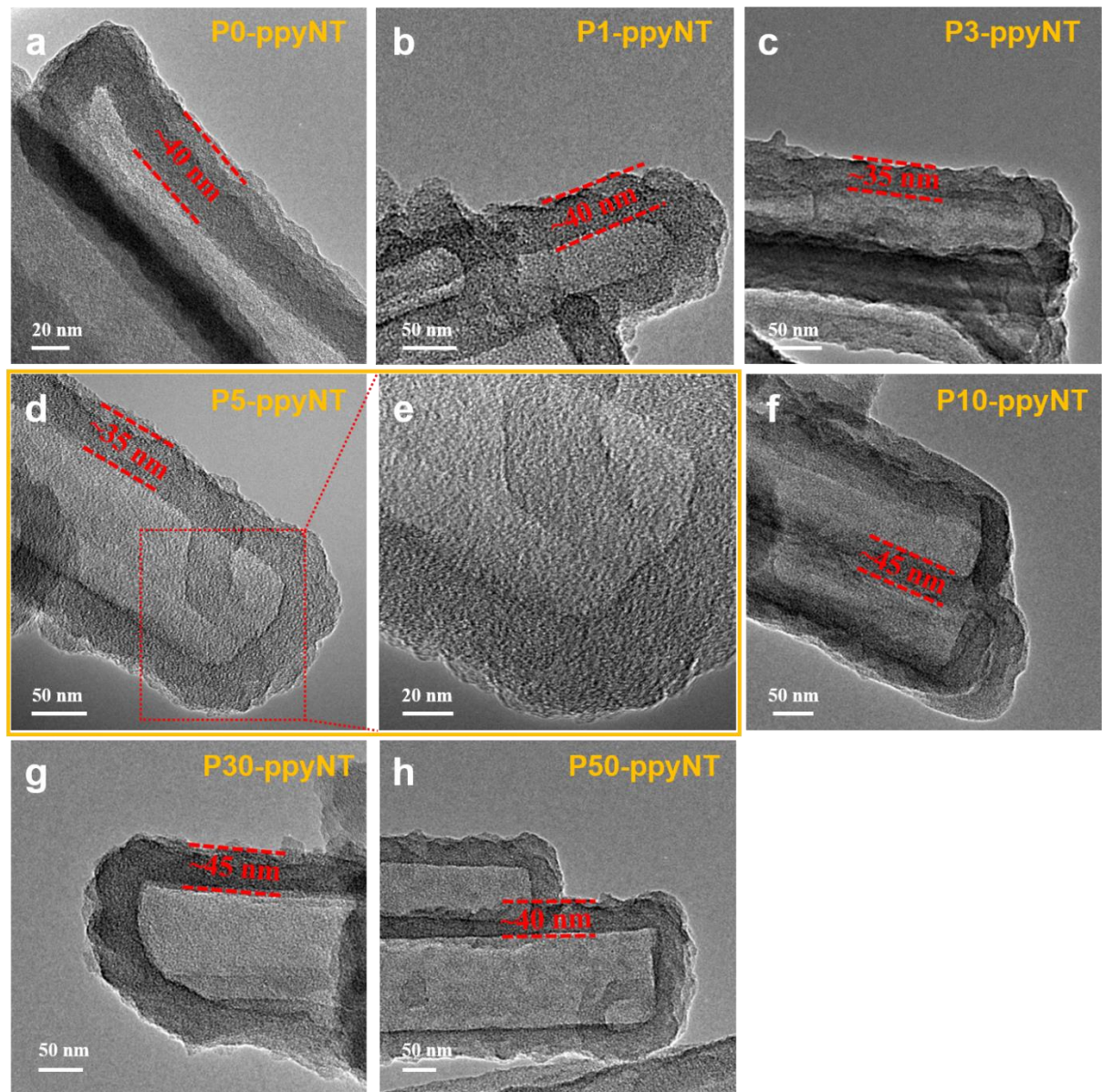


Figure S2. TEM analysis for wall thickness and hollow cavity of (a) P0-ppyNT; (b) P1-ppyNT; (c) P3-ppyNT (d) P5-ppyNT and (e) corresponding high-resolution TEM image; (f) P10-ppyNT; (g) P30-ppyNT; (h) P50-ppyNT.

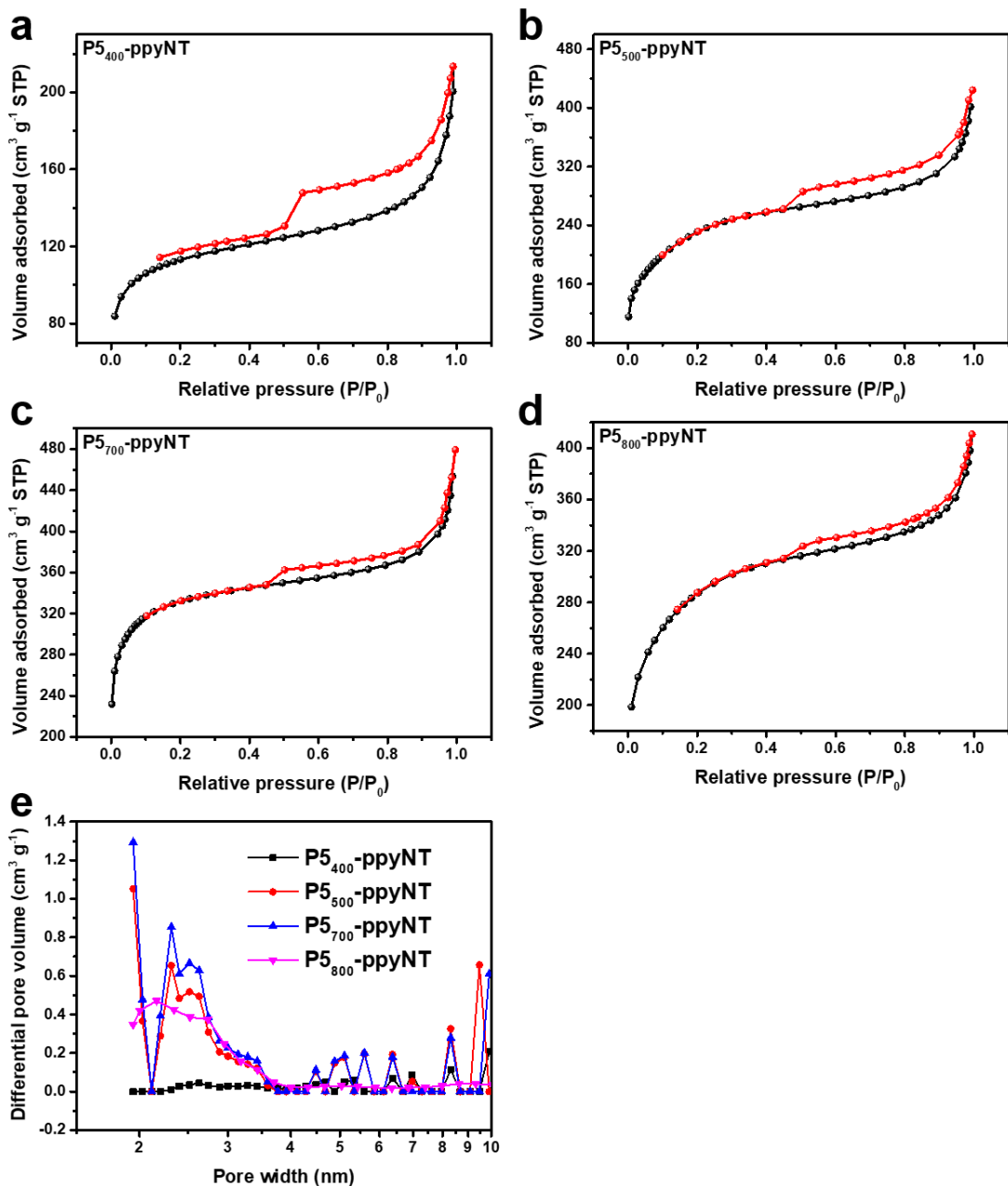


Figure S3. N_2 adsorption/desorption isotherms of (a) $\text{P5}_{400}\text{-ppyNT}$; (b) $\text{P5}_{500}\text{-ppyNT}$; (c) $\text{P5}_{700}\text{-ppyNT}$; (d) $\text{P5}_{800}\text{-ppyNT}$ and (e) the related pore size distribution curves.

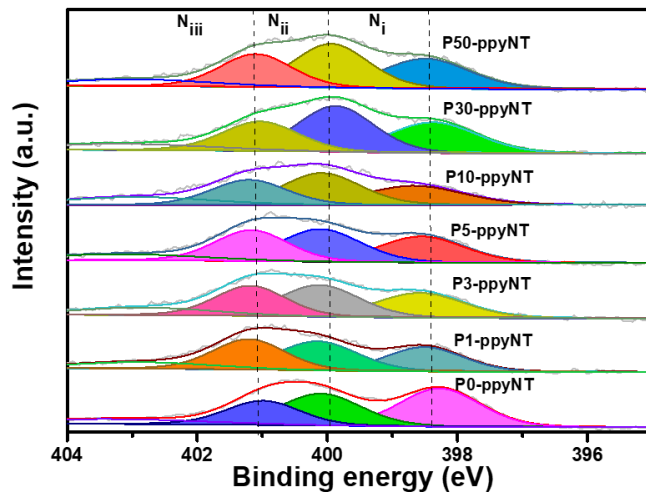


Figure S4. High-resolution N 1s spectra of Px-ppyNT samples.

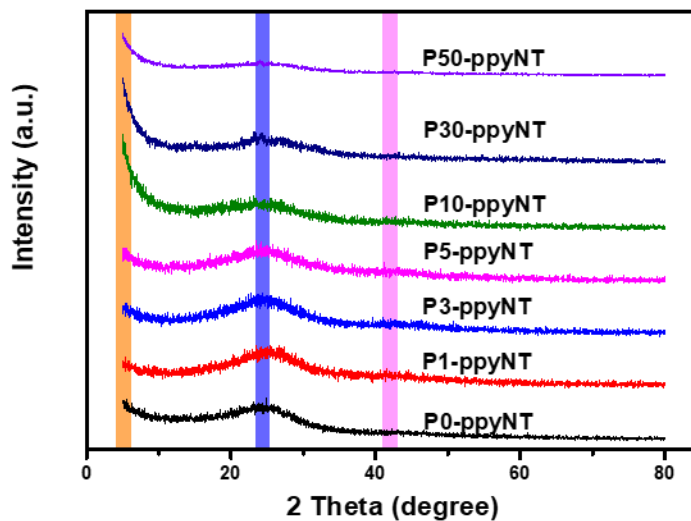


Figure S5. XRD patterns of Px-ppyNT samples. The three bands at $\sim 5^\circ$, $\sim 24.2^\circ$ and $\sim 43^\circ$ represent the preserved porous structure after thermalization, stacked graphitic-like systems and in-plane aromatic systems, respectively.

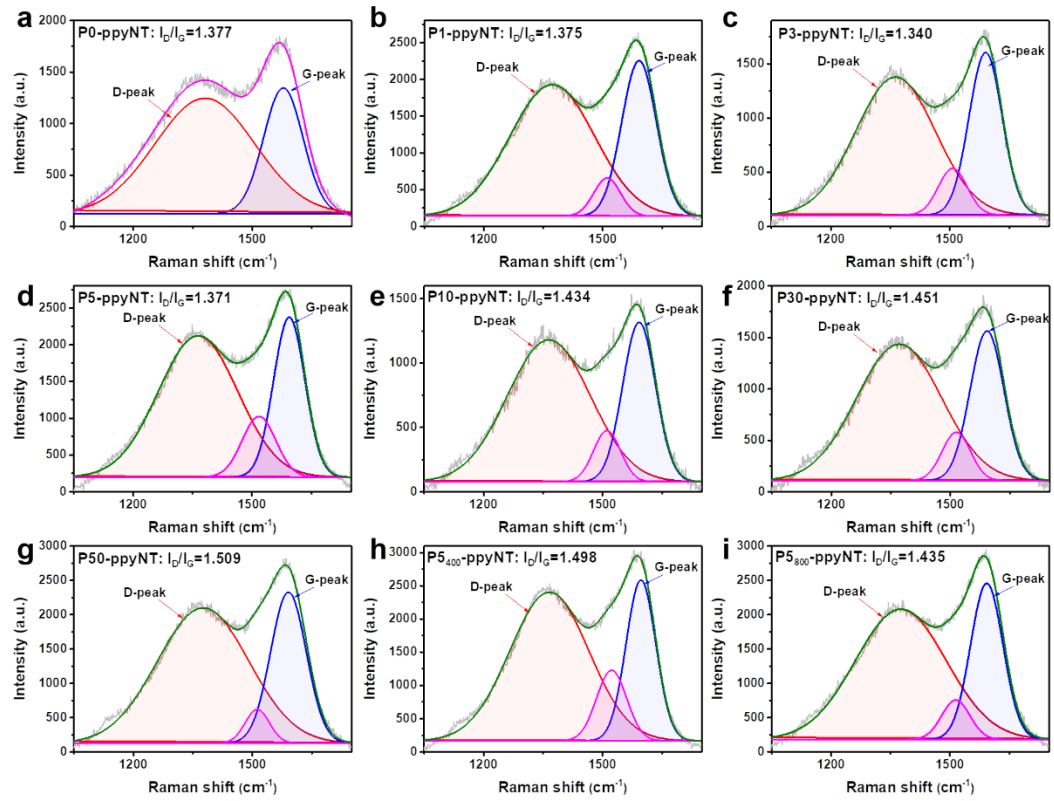


Figure S6. Background-subtracted and deconvoluted Raman spectra of Px-ppyNT samples.

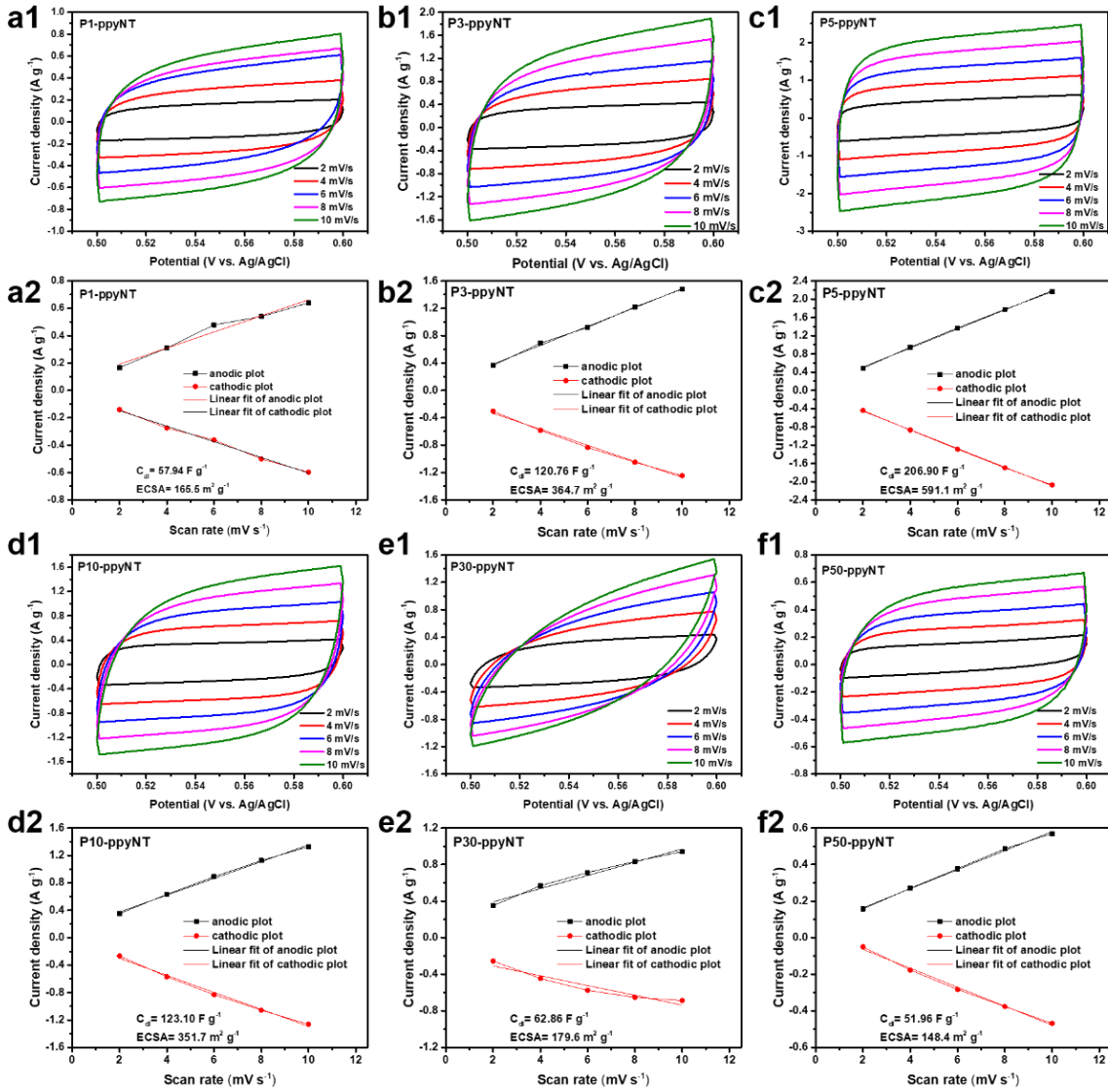


Figure S7. (a1, b1, c1, d1, e1 f1) CV curves at different scan rates and (a2, b2, c2, d2, e2, f2) the cathodic and anodic charging current densities measured at 0.55 V vs Ag/AgCl plotted as a function of scan rate.

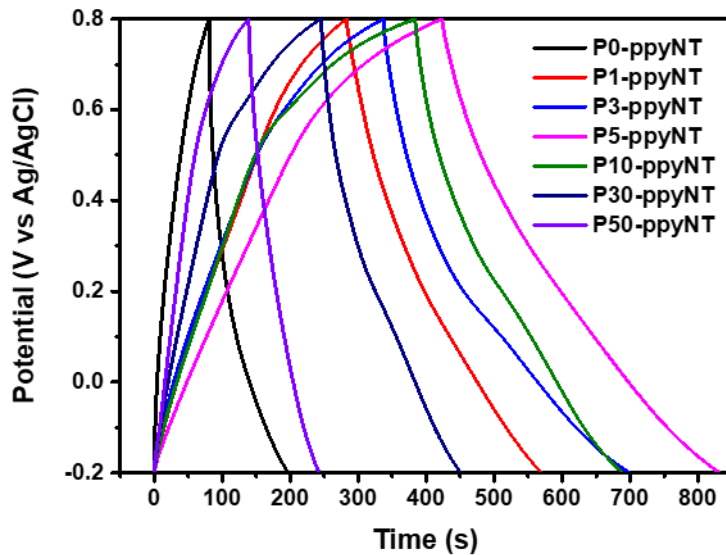


Figure S8. GCD curves of Px-ppyNT at 1 A g^{-1} .

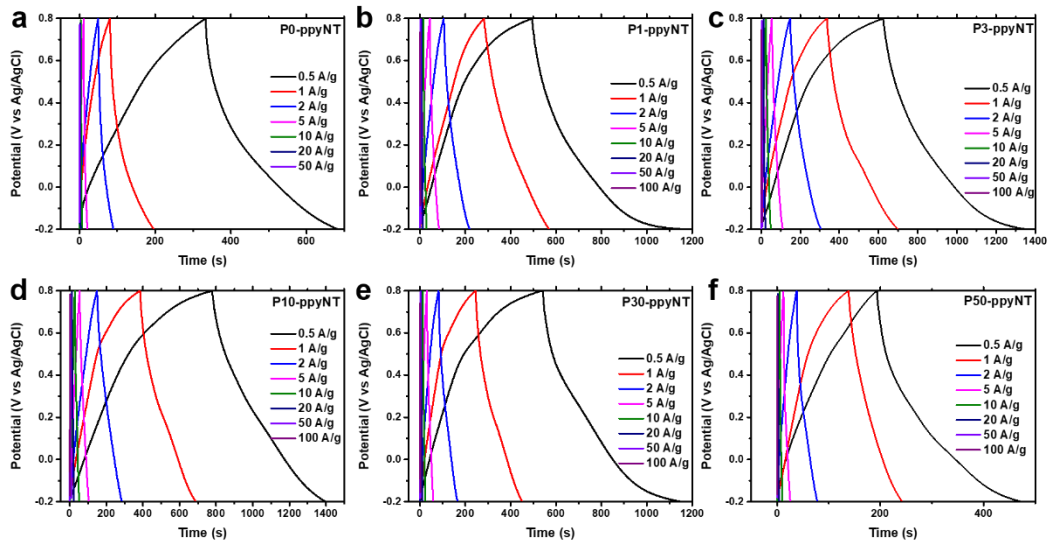


Figure S9. Galvanostatic charge-discharge curves at different current densities of Px-ppyNT samples in a three-electrode system in $1 \text{ M H}_2\text{SO}_4$.

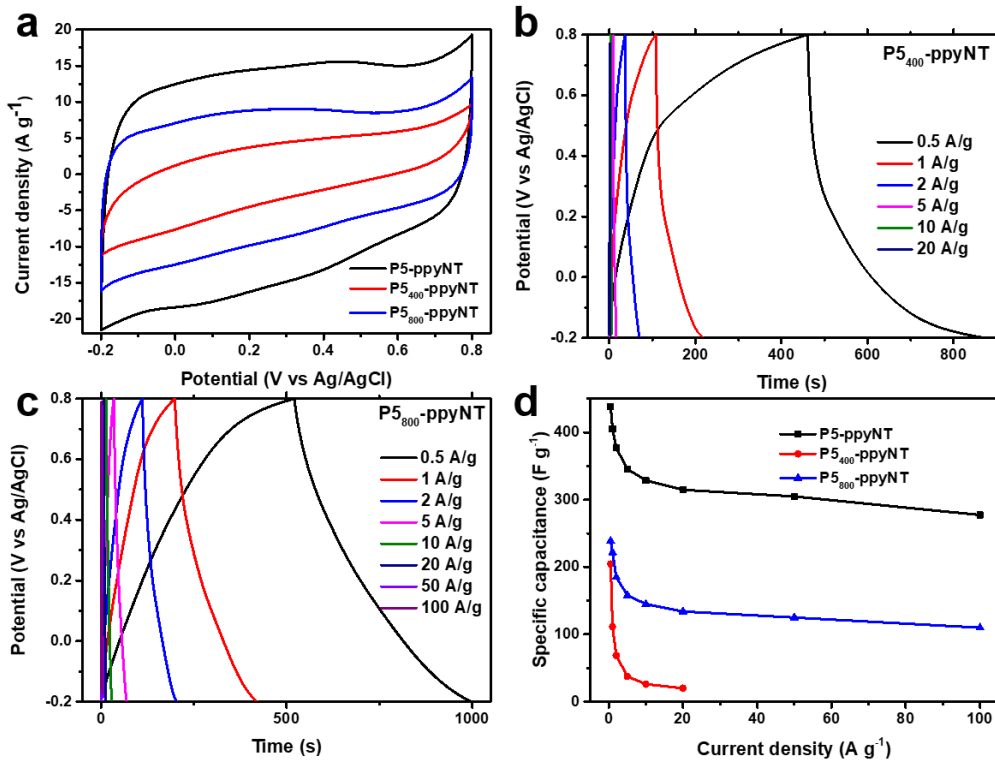


Figure S10. Comparison of electrochemical performance for P5-ppyNT, P5₄₀₀-ppyNT and P5₈₀₀-ppyNT. (a) CV curves at 50 mV s⁻¹; GCD curves of (b) P5₄₀₀-ppyNT and (c) P5₈₀₀-ppyNT at different current densities; (d) rate performance in a three-electrode system in 1 M H₂SO₄.

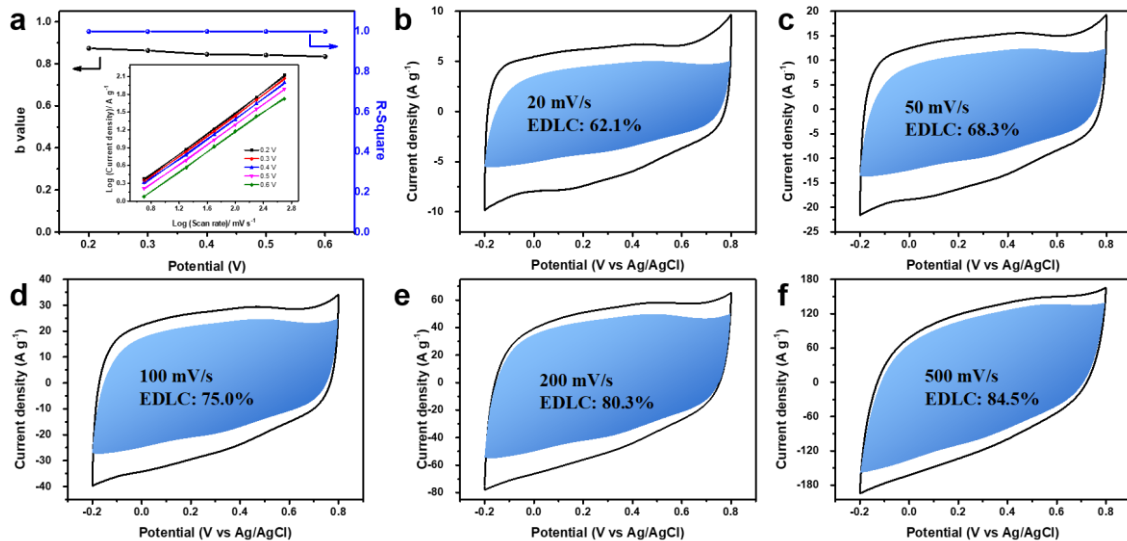


Figure S11. (a) b values against potentials (inset is the plots of current response against scan rate at different potentials); (b)-(f) CV curves of P5-ppyNT with decoupled contribution of EDLC and pseudocapacitive capacitance at different scan rates.

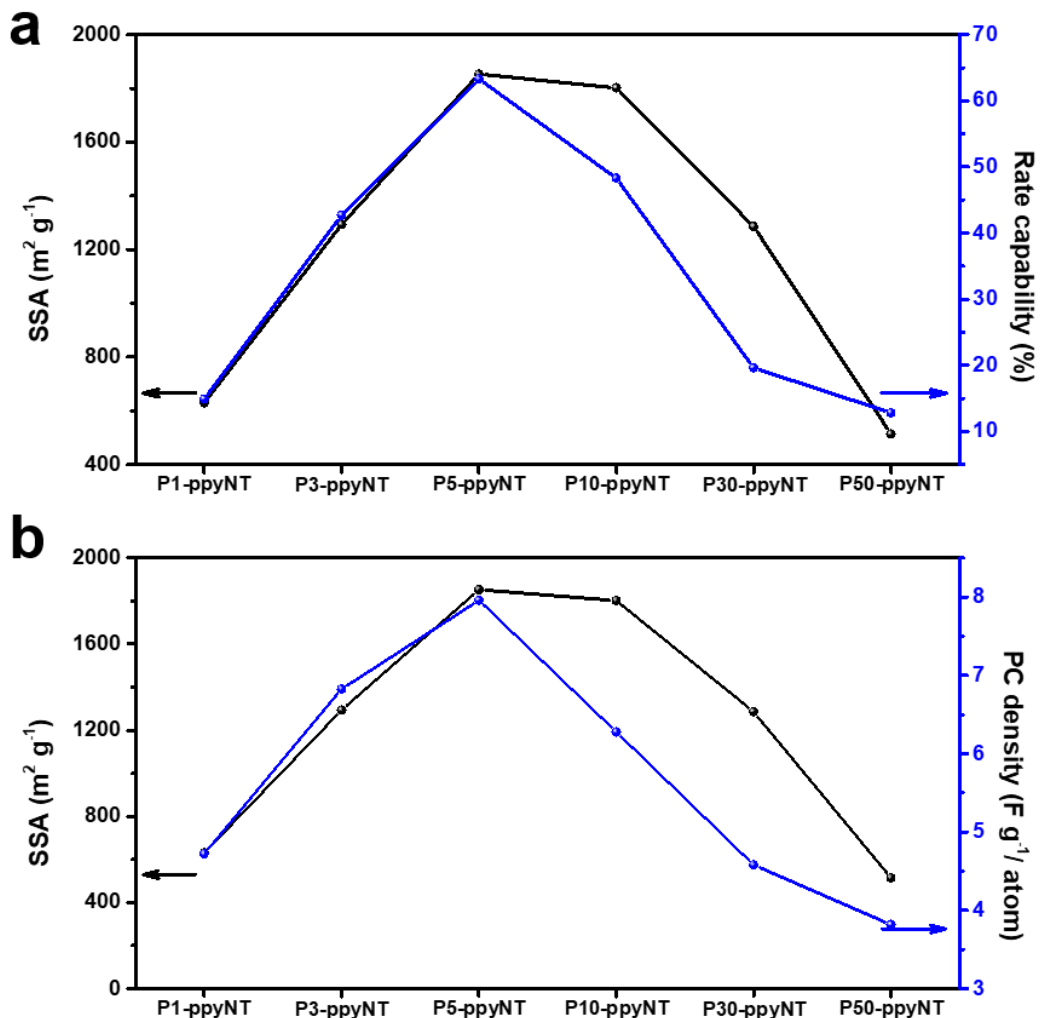


Figure S12. (a) Relationship between the SSA and rate capability; (b) relationship between the SSA and PC density.

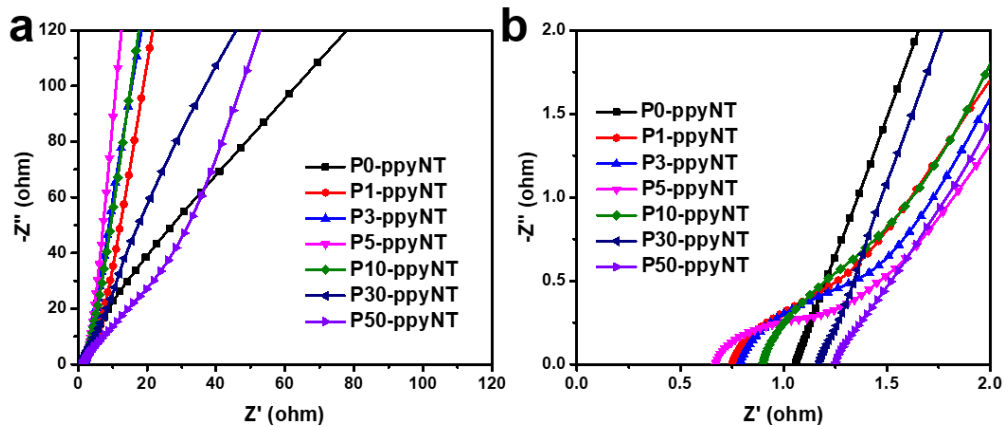


Figure S13. (a) Nyquist plots and (b) the magnified high-frequency region of P_x -ppyNT samples.

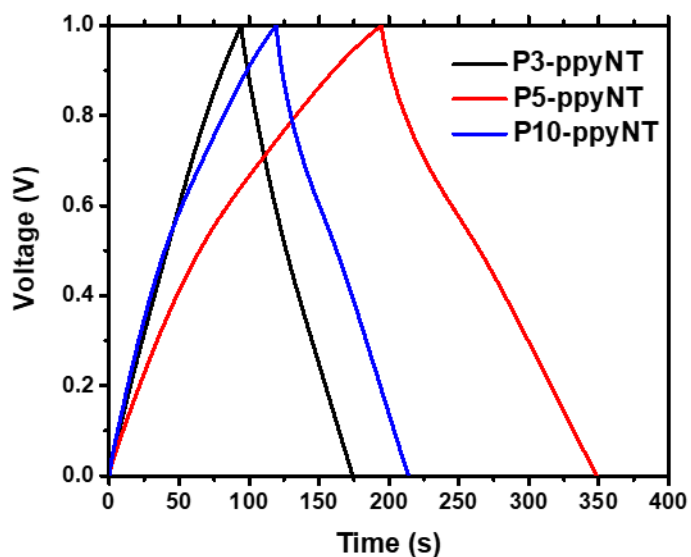


Figure S14. GCD curves of P3-ppyNT, P5-ppyNT and P10-ppyNT in two electrode system at 1 A g^{-1} in $1\text{M H}_2\text{SO}_4$.

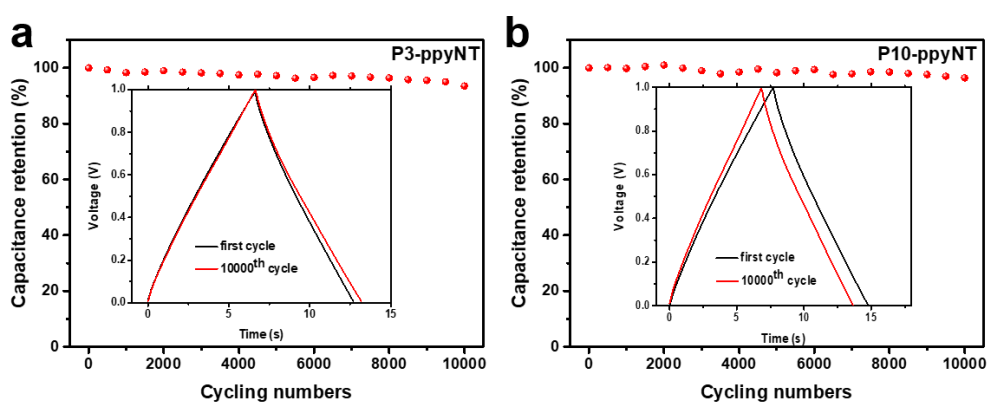


Figure S15. Long-term cycling performance of P3-ppyNT and P10-ppyNT measured at 10 A g⁻¹ over 10000 cycles in two electrode system in 1M H₂SO₄.

Table S1. Comparison of SSA and specific capacitance of related 1D carbon nanomaterials and P5-ppyNT reported in this work.

Sample name	SSA ($\text{m}^2 \text{ g}^{-1}$)	Specific capacitance (F g^{-1})	Reference
1D hierarchically porous carbon (1D-HPC)	1394	256.5 (at 5 mV s^{-1})	[1]
1D carbon nanobelts (CNB)	1208	262 (at 0.5 A g^{-1})	[2]
Carbon nanorods	1,559	164 (at 10 mV s^{-1}) ^{a)}	[3]
Hierarchical porous carbon nanorods (HPCR)	1100.9	274 (at 0.5 A g^{-1})	[4]
1D CNT@micro-C	1306	243 (at 0.5 A g^{-1}) ^{b)}	[5]
Mesoporous carbon nanofibers	1218	276 (at 0.5 A g^{-1})	[6]
Nitrogen and fluorine doped mesoporous carbon nanofibers (NFMCNFs)	596.1	252.6 (at 0.5 A g^{-1})	[7]
P5-ppyNT	1853	438 (at 0.5 A g^{-1})	This work

a, b): Tested as two-electrode symmetrical supercapacitor cell.

Table S2. Detailed SSA, pore volume, I_D/I_G values and ECSA of Px-ppyNT samples.

samples	$S_{BET} (m^2 g^{-1})$	$S_L (m^2 g^{-1})$	Pore volume ($cm^3 g^{-1}$)	I_D/I_G	ECSA($m^2 g^{-1}$)
P0-ppyNT	44	61	0.06	1.377	--
P1-ppyNT	630	840	0.37	1.375	165.5
P3-ppyNT	1294	1723	0.73	1.340	364.7
P5-ppyNT	1853	2563	1.11	1.371	591.1
P10-ppyNT	1802	2474	1.07	1.434	351.7
P30-ppyNT	1286	1776	0.78	1.451	179.6
P50-ppyNT	514	710	0.40	1.509	148.4
P5 ₄₀₀ -ppyNT	390	520	0.27	1.498	--
P5 ₈₀₀ -ppyNT	1004	1359	0.59	1.435	--

Table S3. Elemental composition of Px-ppyNT samples from XPS results.

samples	Element composition (at.%)				
	C	P	N	O	S
P0-ppyNT	84.291	-	11.245	4.372	0.092
P1-ppyNT	81.946	1.386	6.298	9.965	0.404
P3-ppyNT	81.129	2.220	6.666	9.725	0.261
P5-ppyNT	78.732	2.514	7.168	11.450	0.137
P10-ppyNT	78.659	2.752	5.661	12.928	-
P30-ppyNT	76.441	3.374	6.873	13.312	-
P50-ppyNT	74.581	3.855	8.193	13.370	-
P5 ₄₀₀ -ppyNT	77.119	2.421	6.247	13.815	0.399
P5 ₈₀₀ -ppyNT	82.139	1.455	3.249	12.887	0.270

Table S4. Calculated ratio of Nx in Px-ppyNT samples.

samples	Ratio of Nx (%)			
	Ni	Nii	Niii	Niv
P0-ppyNT	37.27	31.00	21.23	10.49
P1-ppyNT	25.79	31.77	29.80	12.64
P3-ppyNT	27.91	31.97	26.93	13.20
P5-ppyNT	27.71	32.55	27.96	11.79
P10-ppyNT	25.20	33.45	25.43	15.91
P30-ppyNT	29.08	36.52	23.37	11.02
P50-ppyNT	28.27	35.21	25.35	11.17
P5 ₄₀₀ -ppyNT	26.84	45.65	20.55	6.96
P5 ₈₀₀ -ppyNT	21.02	45.61	27.45	5.92

Table S5. Calculated ratio of P species in Px-ppyNT samples.

samples	Ratio of P species (%)		
	P 1 (C 3 -P=O)	P 2 (C-P-O)	P 3 (C-O-P)
P1-ppyNT	30.30	38.78	30.92
P3-ppyNT	28.83	41.24	29.93
P5-ppyNT	33.20	39.73	27.07
P10-ppyNT	35.09	38.27	26.64
P30-ppyNT	36.83	37.64	25.53
P50-ppyNT	33.05	40.93	26.02
P5 ₄₀₀ -ppyNT	28.54	42.23	29.23
P5 ₈₀₀ -ppyNT	44.90	21.58	33.52

Table S6. Calculated rate capability, PC density and heteroatom ratio of Px-ppyNT.

Samples	Rate capability (%)	PC density (F g ⁻¹ atom ⁻¹)	Heteroatom ratio (at%)
P1-ppyNT	14.9	4.72	18.054
P3-ppyNT	42.7	6.82	19.871
P5-ppyNT	63.3	7.96	21.268
P10-ppyNT	48.3	6.28	21.341
P30-ppyNT	19.6	4.58	23.559
P50-ppyNT	12.8	3.82	25.419

References

- [1] Liang, C.; Bao, J.; Li, C.; Huang, H.; Chen, C.; Lou, Y.; Lu, H.; Lin, H.; Shi, Z.; Feng, S. One-dimensional hierarchically porous carbon from biomass with high capacitance as supercapacitor materials. *Micropor. Mesopor. Mat.* **2017**, *251*, 77-82.
- [2] Ouyang, T.; Cheng, K.; Yang, F.; Zhou, L.; Zhu, K.; Ye, K.; Wang, G.; Cao, D. From biomass with irregular structures to 1D carbon nanobelts: a stripping and cutting strategy to fabricate high performance supercapacitor materials. *J. Mater. Chem. A* **2017**, *5*, 14551-14561.
- [3] Pachfule, P.; Shinde, D.; Majumder, M.; Xu, Q. Fabrication of carbon nanorods and graphene nanoribbons from a metal-organic framework. *Nat. Chem.* **2016**, *8*, 718-724.
- [4] Fang, L.; Xie, Y.; Wang, Y.; Zhang, Z.; Liu, P.; Cheng, N.; Liu, J.; Tu, Y.; Zhao, H.; Zhang, J. Facile synthesis of hierarchical porous carbon nanorods for supercapacitors application. *Appl. Surf. Sci.* **2019**, *464*, 479-487.
- [5] Li, Z.; Li, L.; Li, C.; Zhong, W.; Zhang, H. Construction of Hierarchically One-Dimensional Core-Shell CNT@Microporous Carbon by Covalent Bond-Induced Surface-Confined Cross-Linking for High-Performance Supercapacitor. *ACS Appl. Mater. Interfaces* **2017**, *9*, 15557-15565.
- [6] Zhang, X.-Q.; Sun, Q.; Dong, W.; Li, D.; Lu, A.-H.; Mu, J.-Q.; Li, W.-C. Synthesis of superior carbon nanofibers with large aspect ratio and tunable porosity for electrochemical energy storage. *J. Mater. Chem. A* **2013**, *1*, 9449-9455.
- [7] Na, W.; Jun, J.; Park, J. W.; Lee, G.; Jang, J. Highly porous carbon nanofibers co-doped with fluorine and nitrogen for outstanding supercapacitor performance. *J. Mater. Chem. A* **2017**, *5*, 17379-17387.